a means to this end, then one must be able to associate to this system a local permeability and permittivity with negative values that keep an analogy with those of an effective medium, in other words, both the effective ϵ and μ should depend on the frequency ω only, and not on the components of the wavevector. This is not at all obvious from the combination of the metallic circuit elements [17].

Concerning superlenses with complex media constituting negative index slabs, we prove that amplified waves inside ideally lossless, dispersiveless negative index media are limited to a penetration depth equal to the focusing distance inside such slabs, and hence no superfocusing including evanescent components can be obtained. In addition, the presence of absorption is very difficult to overcome, it easily transforms amplified components of the wavefield into decaying ones.

Acknowledgements

Work supported by the Spanish DGICYT.

References

1. Veselago, V.G. (1968) Sov. Phys. Usp. 10, 509.
2. Pendry, J.B., Holden, W., Stewart, W., and Youngs, I. (1996) Phys. Rev. Lett. **76**, 4773.
3. Pendry, J.B. (2000) Phys. Rev. Lett. **85**, 3966.
4. Valanju, P.M., Walser, R.M., and Valanju, A.P. (2002) Phys. Rev. Lett. **88**, 187401-1.
5. Garcia, N. and Nieto-Vesperinas, M. (2002) Opt. Lett.**27**, 885.
6. Garcia, N. and Nieto-Vesperinas, M. (2002) Phys. Rev. Lett. **88**, 207403.
7. Shelby, R.A., Smith, D.R., Nemat-Nasser, S.C., and Scultz, S. (2001) Appl. Phys. Lett. **78**, 489.
8. Shelby, R.A., Smith, D.R., and Schultz, S. (2001) Science **292**, 77.
9. Ponizovskaya, E.V., Nieto-Vesperinas, M., and Garcia, N., Appl. Phys. Lett. **81**, 4470 (2002).
10. Landau, L.D. and Lifshitz, E.M. (1963) *Electrodynamics of Continuous Media*, Pergamon Press, Oxford.
11. Born, M. and Wolf, E. (1999) *Principles of Optics*, 7th Edition, Cambrige University Press, Cambridge.
12. Boas, R.P. (1954) *Entire Functions*, Academic Press, New York; Nieto-Vesperinas, M. (1991), *Scattering and Diffraction in Physical Optics*, J. Wiley, New York; Wolf, E. and Nieto-Vesperinas, M. (1985) J. Opt. Soc. Am. **A 2**, 886.
13. t'Hooft, G.V. (2001) Phys. Rev. Lett. **87**, 249701; Williams, J.M. (2001) *Phys. Rev. Lett.* **87**, 249703.
14. Mandel, L. and Wolf, E. (1995) *Optical Coherence and Quantum Optics*, Cambridge University Press, Cambridge.
15. Sherman, G.C. and Bremermann, H.J. (1969) J. Opt. Soc. Am. **59**, 146.
16. Cohen-Tannoudji, C., Diu, B., and Laloe, F. (1977) *Quantum Mechanics*, J. Wiley, New York.
17. Simovski, C.R., Below, P.A., and He, S., IEEE Trans. Antennas Propag., in press (see also arXiv: cond-mat/0211205).

LOCAL FIELD STATISTIC AND PLASMON LOCALIZATI IN RANDOM METAL-DIELECTRIC FILMS

DENTCHO A. GENOV, ANDREY K. SARYCHEV AND VLADIMIR M. SHALAEV
School of Electrical and Computer Engineering, Purdue University, West Lafayette, Indiana 47907-1285

Abstract. A new, exact and efficient numerical method for calculating effective conductivity and local-field distributions in random *R–L–C* works is developed. Using this method, the local field properties of ran metal dielectric films are investigated in a wide spectral range and for a ety of metal concentrations p. It is shown that for metal concentrations to the percolation threshold ($p = p_c$) and frequencies close to the resona the local field intensity is characterized by a non-Gaussian, exponent broad distribution. For low and high metal concentrations a scaling regi formed that is due to the increasing number of non-interacting dipoles. local electric fields are studied in terms of characteristic length parame Properties of both localized and extended eigenmodes in the Kirchh Hamiltonian are investigated.

1. Introduction

The last two decades was a time of immense improvement in our un standing of the optical properties of inhomogeneous media [1]. One of important representatives of such media is a metal-dielectric compo near the percolation threshold. This type of nanostructured materials attracted recently lots of attention because of their unique electromagn properties. Many fundamental phenomena, such as localization and c calization of electrons and optical excitations, play an important rol random media. The light-induced plasmon modes in metal-dielectric c posites can result in dramatic enhancement of optical responses in a br spectral range. In particular, percolation metal-dielectric films can be ployed for surface-enhanced spectroscopy with unsurpassed sensitivity

for development of novel optical elements, such as optical switches and efficient optical filters, with transparency windows induced by local photomodification in the composite films.

In the optical and infrared spectral ranges, the metal dielectric permittivity has, typically, a negative real part, so that metal particles can be viewed as inductance elements with small losses (R–L elements). In accordance with this assumption, a metal-dielectric composite can be treated as an R–L–C network, where the C elements stand for dielectric grains, which have a positive dielectric permittivity. Many different approaches based on the effective-medium theories and various numerical models have been suggested to describe the optical nonlinearities of such systems [2]. In particular, a number of numerical simulations have been carried out by using the real space renormalization group [3–8]. A recently developed scaling theory [4–8] for the field fluctuations and high-order field moments predicts localization of the surface plasmons in percolation composites and strong enhancement for the local field, resulting from the localization. Experimental observations [7, 9] in accord with the theoretical predictions show the existence of giant local fields, which can be enhanced by a factor of 10^5 for the linear response and 10^{20} and greater for the nonlinear response. A recent study [10] of the plasmon modes in metal-dielectric films gives more insights into the problem. Thus, in Ref. [10] it was found that for all studied systems the local fields are concentrated in nanometer size areas, while some of the eigenstates are not localized.

Despite the progress, computer modeling of the electric field distribution in metal-dielectric nanocomposites was restricted so far to mainly approximate methods, such as the real space renormalization group (RSRG). To some extent, this was justified since the focus of those calculations was on the effective properties, such as the macroscopic conductivity and dielectric permittivity. Many fast algorithms were suggested for determining the effective conductivities; those include very efficient models, such as Frank and Lobb $Y - \nabla$ transformation [11], the exact numerical renormalization in a vicinity of the percolation threshold [12–14], and the transfer matrix method [15]. Unfortunately, all these methods cannot be used for precise calculation of the local-field distribution and a new approach is needed. The relaxation method (RM) was one of the first algorithms to give some insight into the field distributions [16]. This method has the advantage of using the minimum possible memory, which is proportional to the number of the sites, L^d, where L is the size of the system and d is the space dimensionality. The fast Fourier acceleration [17] allows one to perform calculations for both $2D$ and $3D$ percolation systems. However, the "critical slowing down" effect and the problem of stability (occurring when the imaginary part of the local conductivity takes both positive and negative values) restricts the use of this approach. Thus, the local-field statistic percolation composites in the optical and infrared spectral ranges wa investigated until very recently, with direct numerical methods not in ing any *a priori* assumptions. In their work, Zekri, Bouamrane, and [18] suggested a substitution method, which allows one to calculate the field distributions in percolation metal-dielectric composites in the op range. However, results obtained for the local-field intensity $I = |E|^2$ d bution function $P(I)$ appear to be rather surprising. Specifically, inste the predicted theoretically and observed experimentally enhancemen the local field, the authors of Ref. [18] obtained average local field int ties far less than the applied field. We note that the high local fields a crucial role in enhancement for nonlinear optical effects and thus important to verify this prediction by exact calculations.

In this work we apply a new numerical method, which we refer t block elimination (BE) [19]. The BE method allows calculations of e tive parameters (such as the conductivity, dielectric permittivity, etc.) most importantly, the local field distribution in inhomogeneous media. focus our attention on the local-field distribution $P(I)$ and compare sults obtained by the BE with those following from the RSRG, the re ation method, and the Zekri-Bouamrane-Zekri (ZBZ) method. Specific we investigate the properties of two-dimensional random metal-diele composites by modeling them as a square lattice with the lattice siz comprised of dielectric and metal bonds, with conductivity σ_d and σ_m spectively. The probability of a bond to have the metal conductivity is equal to p (where p is the metal concentration) while the probab to have the dielectric conductivity σ_d is equal to $1 - p$. We obtain the local electric field is characterized by sharp peaks that can exceed applied field by several orders of magnitude, in agreement with earlier oretical predictions and experimental observations [4–9]. The field max are associated with the localized surface plasmons. For the first time a set of field distribution functions $P(I)$ that gradually transform from "one-dipole" field distribution to the log-normal distribution are calcula by using the newly developed BE method. Relying on an approach ba on the inverse participation ratio, we find important relations for the f correlation length ξ_e, average field localization length ξ_f, and the aver distance between the metal particles ξ_a. The eigenvalue problem is sol directly and effects due to the existence of extended states, predicted [10] are investigated.

2. Block Elimination (BE) Method

In the explanation of the Block Elimination method we will follow the outline introduced in our previous work [19]. We will consider the problem of a local field distribution in nanoscale metal-dielectric films at and away from the percolation threshold. When the wavelength λ of the incident light is much larger than the metal grain size a we can introduce local potential $\varphi(\mathbf{r})$ and local current $\mathbf{j}(\mathbf{r}) = \sigma(\mathbf{r}) \cdot (-\nabla\varphi(\mathbf{r}) + \mathbf{E}_0)$, where $\mathbf{E}_0$ is the applied field and $\sigma(\mathbf{r})$ is the local conductivity. In the quasistatic approximation, the problem of the potential distribution is reduced to solving the current conservation law $\nabla \cdot \mathbf{j}(\mathbf{r}) = 0$, which leads to the Laplace equation $\nabla \cdot [\sigma(\mathbf{r}) \cdot (-\nabla\varphi(\mathbf{r}) + \mathbf{E}_0)] = 0$ for determining the potentials. Now we use the discretization procedure based on the tight-binding model. The film is described as a binary composite of metal and dielectric particles, which are represented by metal and dielectric bonds in the square lattice. The current conservation for lattice site i acquires the following form

$$\sum_j \sigma_{ij}(\varphi_i - \varphi_j + E_{ij}) = 0, \tag{1}$$

where φ_i is the field potential of site i. The summation is over the nearest (to i) neighbor sites j; $\sigma_{ij} = \sigma_{ji}$ are the conductivities of bonds connecting neighbor sites i and j and E_{ij} are the electromotive forces. The electromotive forces E_{ij} are defined so that $E_{ij} = aE_0$, for the bond leaving site i in the "$+y$" direction, and $E_{ij} = -aE_0$, for the bond in the "$-y$" direction; E_{ij} is zero for the "x" bonds. Note that $E_{ij} = -E_{ji}$.

Numerical solution to the Kirchhoff's equations (1) in the case of large lattice sizes encounters immense difficulties and requires very large memory storage and high operational speed. A full set of the Kirchhoff equations for a square lattice of size L is comprised of L^2 separate equations. This system of equations can be written in the matrix form

$$\hat{\mathbf{H}} \cdot \mathbf{\Phi} = \mathbf{F}, \tag{2}$$

where $\hat{\mathbf{H}}$ is a symmetric, $L^2 \times L^2$, matrix that depends on the structure and composition of the lattice, $\mathbf{\Phi} = \{\varphi_i\}$, and $\mathbf{F} = \left\{-\sum_j \sigma_{ij}E_{ij}\right\}$ are vectors of size L^2, which represent the potentials and applied field at each site and bond. In the literature, the matrix $\hat{\mathbf{H}}$ is called the Kirchhoff Hamiltonian (KH) and it is shown to be similar to the Hamiltonian for the Anderson transition problem in quantum mechanics [5, 7–9]. The Kirchhoff Hamiltonian is a sparse random matrix with diagonal elements $H_{ii} = \sum_j \sigma_{ij}$ (where the summation is over all bond conductivities σ_{ij} that connect the i-th site with it neighbors) and nonzero off-diagonal elements $H_{ij} = -\sigma_{ij}$. For detailed description of the KH see the Appendix.

In principle, Eq. (2) can be solved directly by applying the sta Gaussian elimination to the matrix $\hat{\mathbf{H}}$ [20]. This procedure has a ru proportional to $\sim L^6$ and requires a memory space of the order of L^4. S estimations show that the direct Gaussian elimination cannot be a for large lattice sizes, $L > 40$, because of the memory restrictions an run times for all contemporary personal computers. Fortunately, th matrix $\hat{\mathbf{H}}$ has a simple symmetrical structure that allows implemen of block elimination procedure that can reduce significantly the opera time and memory.

In calculations, we can apply the periodic boundary conditions fo "x" and "y" directions; alternatively, we can also impose parallel or electrode-type boundaries. In the case of the periodic boundary condi we suppose that the sites in the first row of the $L \times L$ lattice are conn to the L-th row, whereas the sites of the first column are connected t last column. Then the Kirchhoff's equations for the first site in the row, for example, have the following form

$$\sigma_{1,L}(\varphi_1 - \varphi_L) + \sigma_{1,2}(\varphi_1 - \varphi_2) + \sigma_{1,L^2-L+1}(\varphi_1 - \varphi_{L^2-L+1} - aE_0) + \sigma_{1,L+1}(\varphi_1 - \varphi_{L+1} + aE_0) = 0,$$

where $\sigma_{1,L}$ is the conductivity of the bond connecting the first and the sites in the first row. The $\sigma_{1,2}$ conductivity connects the first and se sites in the first row, σ_{1,L^2-L+1} connects the first site of the first row an first site of the L-th row, $\sigma_{1,L+1}$ connects the first sites of the first and second rows, and the external field E_0 is applied in the "$+y$" direction. N that the $\sigma_{1,L}$ and σ_{1,L^2-L+1} connections are due to the periodic boun conditions in the "x" and "y" directions, respectively.

In Eq. (3) we numerate the sites of the $L \times L$ lattice "row by row", f 1 (for the first site in the first row) to L^2 (for the last site in the L-th r Then, the KH matrix $\hat{\mathbf{H}}$ acquires a block-type structure. As an exam for a system with size $L = 5$, the matrix $\hat{\mathbf{H}}$ takes the following block fo

$$\hat{\mathbf{H}} = \begin{pmatrix} h^{(11)} & h^{(12)} & 0 & 0 & h^{(15)} \\ h^{(21)} & h^{(22)} & h^{(23)} & 0 & 0 \\ 0 & h^{(32)} & h^{(33)} & h^{(34)} & 0 \\ 0 & 0 & h^{(43)} & h^{(44)} & h^{(45)} \\ h^{(51)} & 0 & 0 & h^{(54)} & h^{(55)} \end{pmatrix},$$

where $h^{(jj)}$ are $L \times L$ tridiagonal matrices with diagonal elements $h_{ii}^{(jj)}$ $\sum_k \sigma_{i+(j-1)L,\,k}$ (the summation is over the nearest neighbors of the s $i + (j-1)L$, which are located in the

diagonal matrices $h^{(kl)} = h^{(lk)} (k \neq l)$ connect the k-th row with the l-th row and vice versa. The matrices in the right upper and in the left bottom corners of the KH matrix $\hat{\mathbf{H}}$ are due to the periodical boundary conditions: they connect the top and the bottom rows and the first and the last columns. The explicit forms for the matrices $h^{(jj)}$ and $h^{(kl)}$ are given in the Appendix.

For large sizes L, the majority of the blocks $h^{(ij)}$ are zero matrices and thus Gaussian elimination will be a very inefficient way to solve the system (2). In fact, in a process of elimination of all block elements below $h^{(11)}$ in matrix (4), the only matrix elements that will change are $h^{(11)}$, $h^{(12)}, h^{(22)}, h^{(15)}$ and $h^{(55)}$ with two more elements appearing in the second and last rows. Thus to eliminate the first block column of the KH we can instead of $\hat{\mathbf{H}}$ work with the following $3L \times 3L$ block matrix (recall that in the considered example we choose, for simplicity, $L = 5$):

$$\hat{\mathbf{h}}^{(1)} = \begin{pmatrix} h^{(11)} & h^{(12)} & h^{(15)} \\ h^{(21)} & h^{(22)} & 0 \\ h^{(51)} & 0 & h^{(55)} \end{pmatrix}. \tag{5}$$

Now to eliminate the first block column of matrix $\hat{\mathbf{h}}^{(1)}$ we apply a standard procedure [19], where by using the diagonal elements of block matrix $h^{(11)}$ as pivots we transform $h^{(11)}$ in a triangle matrix $h^{*(11)}$and simultaneously eliminate $h^{(21)}$ and $h^{(51)}$. The elimination of the first column of $\hat{\mathbf{h}}^{(1)}$and respectively $\hat{\mathbf{H}}$ thus requires only L^3 simple arithmetical operations which is to be compared with L^5 operations needed if we work directly with the whole matrix $\hat{\mathbf{H}}$. After the first step of this block elimination is completed the matrix $\hat{\mathbf{H}}$ has the following form:

$$\hat{\mathbf{H}}^{(1)} = \begin{pmatrix} h^{*(11)} & h^{*(12)} & 0 & 0 & h^{*(15)} \\ 0 & h^{*(22)} & h^{(23)} & 0 & h^{(25)} \\ 0 & h^{(32)} & h^{(33)} & h^{(34)} & 0 \\ 0 & 0 & h^{(43)} & h^{(44)} & h^{(45)} \\ 0 & h^{(52)} & 0 & h^{(54)} & h^{*(55)} \end{pmatrix}, \tag{6}$$

where we denote all blocks that have changed in the elimination process by the "$*$" superscript. The two new block elements $h^{(25)}$ and $h^{(52)}$ appeared due to the interactions of the first row with the second and the fifth rows.

As a second step, we apply the above procedure for the minor $\hat{\mathbf{H}}^{(1)}_{11}$ of the matrix $\hat{\mathbf{H}}^{(1)}$ (which now plays the role of $\hat{\mathbf{H}}$), therefore we work again with $3L \times 3L$ matrix:

$$\hat{\mathbf{h}}^{(2)} = \begin{pmatrix} h^{*(22)} & h^{(23)} & h^{(25)} \\ h^{(32)} & h^{(33)} & 0 \\ h^{(52)} & 0 & h^{*(55)} \end{pmatrix}.$$

Repeating with $\hat{\mathbf{h}}^{(2)}$ all operations we performed on $\hat{\mathbf{h}}^{(1)}$ we put $h^{*(}$ the triangular form and eliminate $h^{(32)}$ and $h^{(52)}$. We continue this p dure until the whole matrix $\hat{\mathbf{H}}$ is converted into the triangular form wi elements below the diagonal being zero. The backward substitution triangular matrix is straightforward, namely we obtain first the site p tials in the L-th row (the fifth row, in our example) and then, by calcul the potentials, in the $L-1$ row and so on, until the potentials in all are obtained. The total number of operations needed is estimated as for the described block elimination (BE) method, which is less tha number L^6 needed for Gaussian or **LU** (for symmetric matrixes) elir tion [20]. The BE has operational speed on the same order of magnitu in the transfer-matrix method [15] and the Zekri-Bouamrane-Zekri (method [18]. However, BE allows the calculation of the local fields, a posed to the Franck-Lobb method, and we believe that it is much easi numerical coding when compared to the ZBZ method.

For a Pentium II 450 MHz processor, the run time we observed is g by the formula $T(L) \simeq 3.2 \cdot 10^{-7} \cdot L^4$ s, which for $L = 250$ is less 23 min. For each step of the BE procedure, we need to keep only L^2 matrix $\hat{\mathbf{h}}^{(k)}$) complex numbers in the operational memory and L^3 on a disk. By using the hard drive we do not decrease the speed perform significantly because only L loadings of L^2 numbers are required, i.e. additional operations in total. Note that the BE, similar to the Gaus elimination, is well suited for parallel computing.

We performed various tests to check the accuracy of the BE algori described above. First, the sum of the currents at each site was calcul and the average value $\sim 10^{-14}$ was found; this is low enough to claim the current conservation holds in the method. Our calculations, using standard Gaussian elimination (for small lattice sizes) and the relaxa method (for the case of all positive conductivities), for the effective ductivity and the local field distribution show full agreement with res obtained using the developed block elimination procedure.

3. Results for 2D Parallel and L-type Lattices

In inhomogeneous media, such as metal-dielectric composites, both die tric permittivity $\varepsilon(\mathbf{r})$ and conductivity $\sigma(\mathbf{r}) = -i\omega\varepsilon(\mathbf{r})/4\pi$ depend on position $\mathbf{r}$. When the size of the composite is much larger than the siz inhomogeneities, the effective conductivity σ_e can be intro

cussed above, we model the composite by an R–L–C network and then apply the BE method to find the field potentials at all sites of the square lattice. When the potential distribution is known we can calculate the effective conductivity:

$$\sigma_e \, |\mathbf{E}_0|^2 = \frac{1}{S} \int \sigma(\mathbf{r}) \, |\mathbf{E}(\mathbf{r})|^2 \, d\mathbf{r} \tag{8}$$

where $\mathbf{E}(\mathbf{r})$ and $\mathbf{E}_0$ are the local and the applied fields, respectively (see, e.g., [2]). The integration is performed over the film surface S.

It is well known that the effective DC conductivity for a two component random mixture ($\sigma_m \gg \sigma_d$) should vanish as a power law, when the metal concentration p approaches the percolation threshold p_c, i.e.,

$$\sigma_e \sim \sigma_m (p - p_c)^t, \tag{9}$$

where t is the critical exponent, which was calculated and measured by many authors. In the 2D case, the critical exponent is given by $t = 1.28 \pm 0.03$, according to Derrida and Vannimenus [15], and $t = 1.29 \pm 0.02$, according to Frank and Lob [11]. The value $t = 1.33 \pm 0.03$ was found by Sarychev and Vinogradov [13], who used the exact renormalization group procedure and reached the lattice size $L = 500$ in their simulations. In all cases, the critical exponent t was calculated using the finite-size scaling theory [21]. When the volume fraction p of the conducting elements reaches the percolation threshold p_c, the correlation length increases as $\xi \sim (p - p_c)^{-\nu}$, where $\nu = 4/3$ is the critical exponent for the correlation length [2]. Because the correlation length ξ determines the minimum size of the network, for which it can be viewed as homogeneous, one expects that for $L \ll \xi$, the effective conductivity depends on the system size L. The finite-size scaling theory [22, 23] predicts the following dependence:

$$\sigma_e(L) \sim L^{-t/\nu} f(\eta), \tag{10}$$

where the argument $\eta = L^{1/\nu}(p - p_c)$ depends on the system size L and on the proximity to the percolation threshold p_c. For a self-dual lattice, such as the square lattice considered here, the percolation threshold is known exactly: $p_c = 0.5$. When calculations are carried out for $p = p_c$ there is no need for knowledge of the specific form of the function f in Eq. (10).

We calculate the effective conductivity $\sigma_e(L)$ for different sizes L. In order to improve the statistics for each size L, a number of distinct realizations were performed. Specifically we used 40,000 realizations for $L = 10$; 5,000 realizations for $L = 20$; 1,000 realizations for $L = 60$; and 100 realizations for $L = 150$. The data from our calculations was fit to Eq. (10) and the χ^2 analysis was applied to determine the critical exponents. Thus we found that $t/\nu = 0.96 \pm 0.03$ and $t = 1.28 \pm 0.04$. This result is i agreement with the estimates of Derrida-Vannimenus and Frank-Lol somewhat lower than the $t/\nu = 1.0$ obtained by Sarychev and Vinog Note that the value $t/\nu = 1.0$ is expected for the sizes $L > 300$ tl greater than those we used in our estimates.

4. Local-Field Distribution Function

To further verify the accuracy of the block elimination method, we explicitly the field distribution function, for the case when the c tivities are positive and real numbers (i.e., the dielectric permitti purely imaginary in this case). The local field distribution $P(I)$ w pled in terms of $\log I$, where $I = (|\mathbf{E} - \mathbf{E}_0|/|\mathbf{E}_0|)^2$ is the local field in fluctuation with $|\mathbf{E}_0|^2$ being the intensity of the applied field. If th conductivities σ_d and σ_m are positive (resistor network), we can alsc the relaxation method [17] and compare the results with those ob with the BE procedure. Such a comparison is presented in Fig. 1, the metal concentration is chosen to be equal to the percolation t old $p = p_c$. The distributions obtained with the two exact metho Block Elimination (BE) and the Relaxation Method (RM), are nea same. The minor deviations are due to the differences in the calcu procedures resulting in different round-off errors, and also because c sufficient relaxation times. The local-field intensities are distributed wide range that extends from low filed intensities of the order of I to very high values reaching $I \sim 10^4$.

In the same figure, the field distribution obtained with the real renormalization group (RSRG) method is also shown. Among mc portant results obtained with this non-exact method is the extens the distribution function toward small values of the field intensity I a distortion is obtained for all distributions calculated with this m however, this does not considerably affect the method's applicabil processes depending on the local field moments. The n-th moment field $M_n = \langle |E|^n \rangle / |E_0|^n$ is given by the spatial average over the fil face and thus depends mainly on the local fields with the largest inte Because the RSRG calculations differ from the exact values only fc intensity fields, the method can be used for estimation of the field mo

Although the case of real positive values for the conductivitie considerable interest, more important physical problems arise wh metal conductivity is complex. One special case corresponds to the s plasmon resonance, which plays a crucial role in the optical and ir spectral ranges for metal-dielectric composites. For the two-dimer case, this resonance for individual particles occurs when $\sigma_d = -\sigma_r$

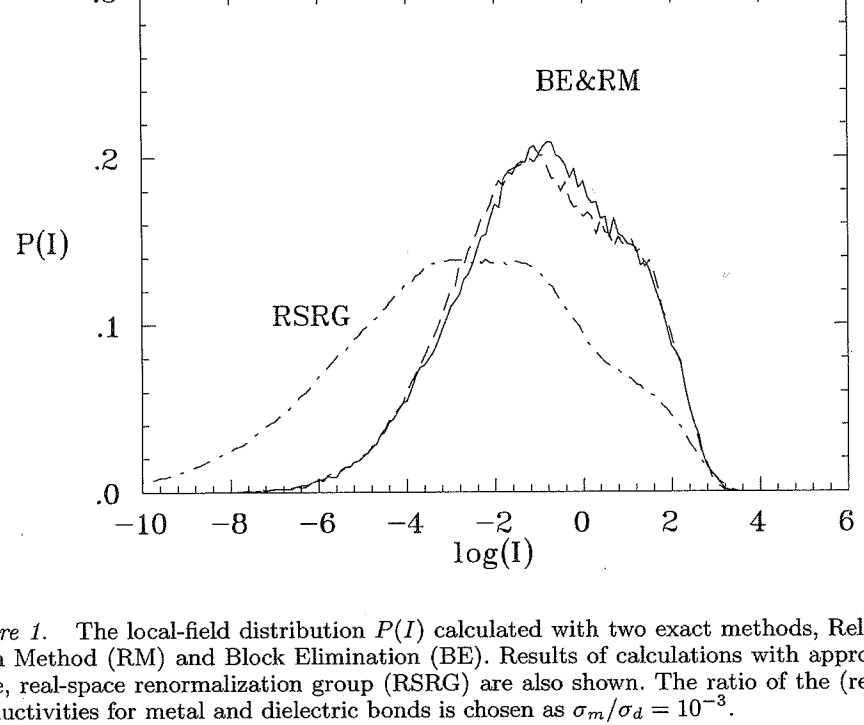

Figure 1. The local-field distribution $P(I)$ calculated with two exact methods, Relaxation Method (RM) and Block Elimination (BE). Results of calculations with approximate, real-space renormalization group (RSRG) are also shown. The ratio of the (real) conductivities for metal and dielectric bonds is chosen as $\sigma_m/\sigma_d = 10^{-3}$.

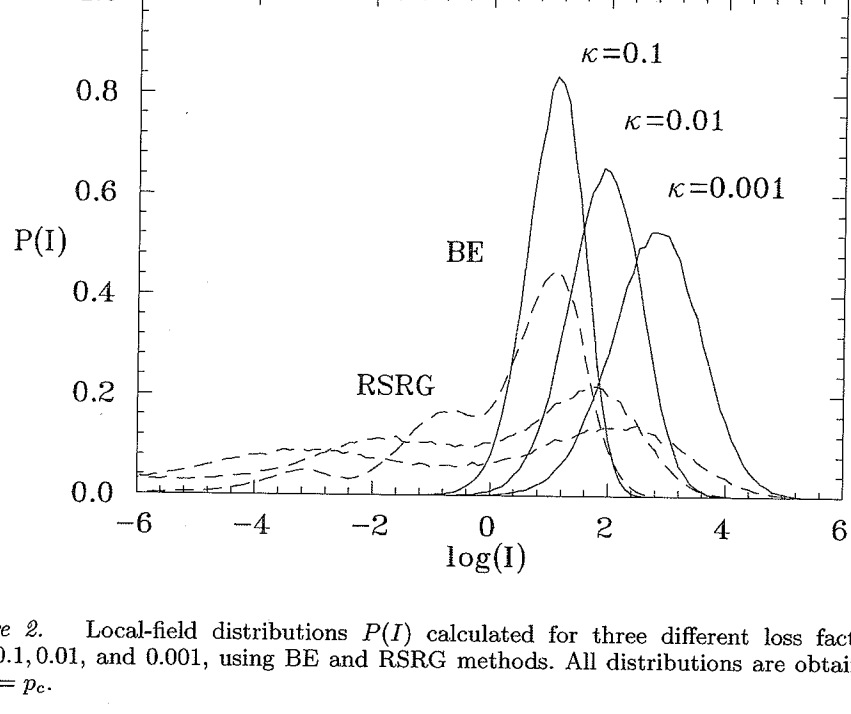

Figure 2. Local-field distributions $P(I)$ calculated for three different loss fact $\kappa = 0.1, 0.01$, and 0.001, using BE and RSRG methods. All distributions are obtai for $p = p_c$.

it can be investigated using a dimensionless set of conductivities $\sigma_d = -i$, and $\sigma_m = i + \kappa$, where $i = \sqrt{-1}$ and κ is a small real conductivity that represents the loses in the system. Recall that in metal-dielectric films the conductivity $\sigma_m = -i\omega\varepsilon_m/4\pi$ is predominantly imaginary with very small real part [23].

In Fig. 2, we show the local-field distributions calculated for three different values of κ, using both the block elimination (BE) and the real space renormalization group (RSRG) procedures. All functions obtained by these two methods differ in shape and peak positions; however, taking into account that the RSRG is indeed an approximate procedure, we can conclude that qualitatively it performs relatively well. All the three local field distributions, which are calculated with the exact BE method, can be approximated by the log-normal function:

$$P(I) = \frac{1}{\Delta I\sqrt{2\pi}} \exp\left[-\frac{(\log I - \langle \log I\rangle)^2}{2\Delta^2}\right], \qquad (11)$$

where $\langle \log I\rangle$ is the average value for the logarithm of the local field intensity I and Δ is the standard deviation in terms of $\log I$ ($\log x \equiv \log_{10} x$).

This approximation for the field distribution seems to work sufficiently w around the average value $\overline{s} = \langle \log I\rangle$. We note, however, that according Ref. [25], where the current distribution was studied, Eq. (11) probably w fail for the intensities I far from the logarithmic average $\overline{s}$. The occurrer of log-normal distribution in a disordered system is related to localizati of plasmon modes. A similar type of dependence was found for the co ductance in the Anderson transition problem [26]. In Fig. 2 we can a see that $\langle \log I\rangle$ and Δ both increase when κ decreases. The increase in t logarithm of the average of the local field can be explained by correlatic between the loss parameter κ and the quality-factor, which leads to relati $\left\langle |E|^2 \right\rangle \sim \kappa^{-1}$ [4]: the smaller the losses, the higher the local fields.

The reference system with $\sigma_d = -i$ and $\sigma_m = i + \kappa$ is an important ca for studying some fundamental properties of metal-dielectric films, but can not be applied for real metals, where σ_m depends on the wavelengt In order to extend our studies to arbitrary materials we can use availab experimental data and theoretical models. For the case of metals, the Dru formula can be used that describes well important characteristics of t

metal permittivity ε_m. The formula is

$$\varepsilon_m(\omega) = \varepsilon_b - (\omega_p/\omega)^2/(1 + i\omega_\tau/\omega), \qquad (12)$$

where ε_b is the contribution due to the inter-band transitions, ω_p is the plasma frequency, and $\omega_\tau = 1/\tau \ll \omega_p$ is the relaxation rate. In our calculations we consider silver-glass film with the following constants: $\varepsilon_d = 2.2$, $\varepsilon_b = 5.0$, $\omega_p = 9.1$ eV, and $\omega_\tau = 0.021$ [28]. In Fig. 3a we show the local field distribution for two different wavelengths: one corresponding to the resonance of individual particles $\omega = \omega_r$, occurring at $\sigma_d = -\sigma_m$ ($\lambda \sim 370$ nm) and another shifted toward longer wavelengths. Again, we observe very wide distributions whose widths increase with the wavelength and enhancement factors reaching values of the order of 10^5. We note that the log-normal approximation Eq. (11) does not hold for frequencies shifted away from the resonance.

The fact that we have extremely high local intensities for wavelengths away from the resonance is remarkable by itself. This effect is due to the interaction of metal particles and it is best manifested at concentrations close to the percolation threshold. A similar long-wavelength spectral behavior was observed in fractal aggregates and is quantitatively explained by the long range character of the dipole-dipole interaction [29]. Because the dipole-dipole interactions are relatively weak, it is expected that for low metal concentrations there should be considerable change in the field distribution. To investigate thoroughly this dependence, we calculated the local field distribution function $P(I)$ for surface metal coverages that deviate from the percolation threshold value. Our results are shown in Fig. 3b where we plot the field distribution for three different metal concentrations: $p = 0.5$, 0.01, and 0.001 at the resonant wavelength $\lambda = 370$ nm. We also include the case of a single metal bond (dipole) positioned in the center of the lattice. The graph shows that there is an apparent transition from the log-normal ($p = p_c$) distribution to a distributions with a "scaling" (power-law) dependence. The appearance of such scaling regions is due to the transformation of the composite film from a strongly coupled dipole system at the percolation threshold into a randomly distributed, sparse configuration of non-interacting dipoles at lower metal concentrations. The range of the scaling interval increases gradually with the decrease of the metal concentration until it "consumes" the entire distribution for the case of a single dipole. In two dimensions, a single dipole placed in the center of the coordinate system induces an electric field with intensity $I_{dip}(r, \theta) = \gamma \cos^2\theta/r^4$, where $r = |\mathbf{r}|$ is the modulus of the radius-vector $\mathbf{r} = \{x, y\}$ and θ is the angle between the field polarization and $\mathbf{r}$. To find the actual one-dipole field distribution $P_{dip}(I)$ we consider the above one-dipole intensity $I_{dip}(r, \theta)$ over the square lattice and then we count the "identical" magnitudes of the logarithm of

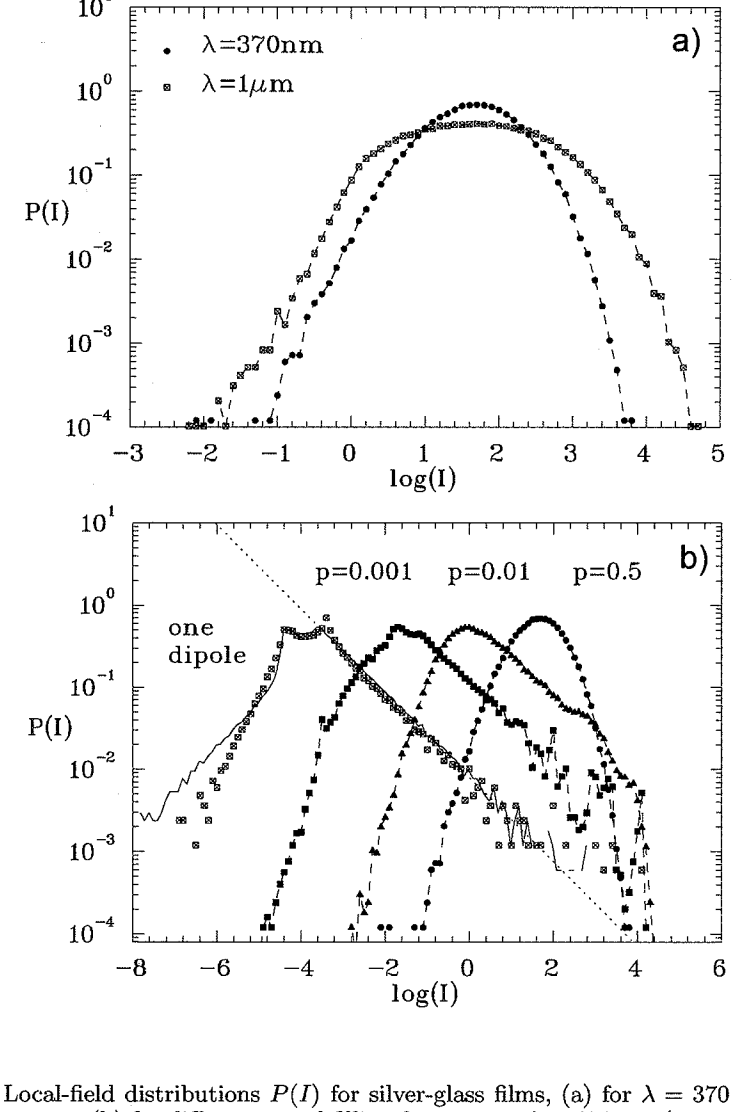

Figure 3. Local-field distributions $P(I)$ for silver-glass films, (a) for $\lambda = 370$ nm $\lambda = 1\mu m$ at $p = p_c$; (b) for different metal filling factors p at $\lambda = 370$ nm (correspond to $\sigma_m = -\sigma_d$).

the field-intensity I. The resultant curve for the one-dipole field distribut (the solid line in Fig. 3b) should be compared with the field distribut obtained by BE calculations for one metal bond positioned in the cente the film. Both distributions match extremely well; it can be seen that method captures even the smallest effects on the distribution caused by cosine term and the square geometry of the lattice. The slope of the scal

region is preserved for all concentrations p and can be fit to the relation $P(I) \sim I^{-\alpha}$, where for the exponent we obtain the value $\alpha = 3/2$. The same relation for the distribution function in the case of a single dipole can be easily derived by calculating the integral $P_{dip}(I) = \iint \delta(I - I_{dip}(r))dS$, where $I_{dip}(r) \sim 1/r^4$, δ is the Dirac delta-function and S represents the film surface. The same universal scaling was also found in fractals [30].

The wide distributions discussed above are probably difficult to observe in experiments. In recent experiments [31, 32], the local filed was measured over the film surface; both studies show local-field distributions $P(I)$ that are well extrapolated by the exponential functions and reach the maximum field enhancement on the order of ~ 50. The strong decrease in the local field intensity and the exponential shape of the distribution is explained by the destructive interference which occurs when the field is collected from an area that is considerably larger then the particle size. By taking into account these interference effects in calculations, it was shown that the theory describes well the experimental data [32].

5. Localization and High-Order Field Moments

One of the most important properties of the metal-dielectric composites is the localization of the surface plasmons. In Ref. [27], the authors performed estimations for surface plasmon localization, using the inverse participation ratio $ipr = (\sum_i^N |\mathbf{E}_i - \mathbf{E}_0|^4)/(\sum_i^N |\mathbf{E}_i - \mathbf{E}_0|^2)^2 = N^{-1}\langle I^2\rangle/\langle I\rangle^2$, where $N = L^d$ it the total number of sites while $\mathbf{E}_i$ is the electric field vector corresponding to i-th site. According to Ref. [27], the ipr for extended plasmons should be size-dependent and characterized by a scale comparable to the size of the system; if there is a tendency to localization, the corresponding exponent should decrease and, for strongly localized fields, it should become unity. For various loss factors κ the authors of [27] found that $ipr \sim L^{-1.3}$ so that the field moment ratio is given as $R = \langle I^2\rangle/\langle I\rangle^2 = ipr \times L^d \sim L^{0.7}$. This result leads to size-dependent field moments which for large L should not be the case. Below we show that the earlier theory [4–8], which is based on Eq. (1), is indeed size-independent and supports the conclusion on plasmon localization with the exact BE method. We will also extract some important relationships that describe statistical properties of the local fields in semicontinuous metal films.

We first focus on the most simple case when there is only one dipole in the entire space. For a single dipole it is easy to obtain the relation $R = \langle I^2\rangle/\langle I\rangle^2 \simeq \frac{1}{3}\varkappa^{\frac{1}{2}}$, where $\varkappa = I_{\max}/I_{\min}$ is the ratio of the maximum (close to the particle) and minimum (away from the particle) in the field intensities. Because of the power-law dependence $I_{dip} \sim r^{-4}$, there is a size-dependence $R \sim \frac{1}{3}(l/a)^2 = \frac{1}{3}L^2$, where l is the length scale of space that is under consideration and a is the average particle size. The s dependence for the one-dipole local-field moments is an expected res since the weight of the low-magnitude fields becomes progressively lar with the increase of the film surface. However, for practical applications, are interested in systems with large numbers of particles so that they c be viewed as macroscopically homogeneous. We can write this condition $n_a = (l/\xi_a)^d \gg 1$, or $(aL/\xi_a)^d = pL^d \gg 1$, where p is the volume fract and ξ_a is the average distance between the metal particles. Now for theory to be size-independent ($R(L) \sim$ const) the condition $L \gg p^{-1/d}$ to be enforced.

By investigating the dynamics of the field moments ratio R we c also determine relationships between important statistical quantities, su as field correlation length ξ_e and field localization length ξ_f. By the fi correlation length ξ_e, we understand the average distance between field peaks, while we characterize their spatial extension by the field calization length ξ_f [23]. For non-overlapping peaks, one can find th $R = N/(N_e N_F) = (\xi_e/\xi_f)^d$, where $N = (l/a)^d = L^d$ is the total nu ber of sites, $N_e = (l/\xi_e)^d$ is the total number of the field peaks, each c occupying $N_F = (\xi_f/a)^d$ sites. In general, for $L \gg p^{-1/d}$, we expect R be a function of p (but not of L) and κ; the same is true for the statisti length ξ_e.

To determine this dependence we run calculations for two loss facto $\kappa = 0.1$ and $\kappa = 0.01$. As illustrated in Fig. 4, for both cases, R can approximated as:

$$R(\kappa, p) = \eta(\kappa)\left\{\left[\theta(p) - \theta(p - \frac{1}{2})\right] p^{-\tau} + \theta(p - \frac{1}{2})(1-p)^{-\tau}\right\}, \qquad (1$$

where θ is the step-function. For the exponent τ, we obtain the value whi is close to the ratio 2/3. For $p \leq 0.5$ and $d = 2$ this value yields t following relationship for the field correlation length: $\xi_e \simeq \xi_f p^{-1/3}\sqrt{\eta(\kappa)}$ $\xi_f(\xi_e/a)^{2/3}\sqrt{\eta(\kappa)}$, where the function $\eta(\kappa)$ increases when κ decreases. T analysis of the ratio ξ_e/ξ_f shows that we should expect an increase of t localization strength with a decrease of both surface coverage p and lo factor κ. In the special case of a single dipole we have $R = (\xi_e/\xi_f)^2 = \frac{1}{3}I$ which, combined with $\xi_e = aL$, yields for the field localization length ξ_f $a\sqrt{3}$.

The localization of the electric filed into "hot" spots can be easily se in Fig. 5, where we show (for different wavelengths) the spatial distributi of the local intensity $I(\mathbf{r})$, and the fourth moment of the local fields, I^2 (Note, that $I^2(\mathbf{r})$ is proportional to the local Raman scattering provid that Raman-active molecules are covering the film [7]. As mentioned, re

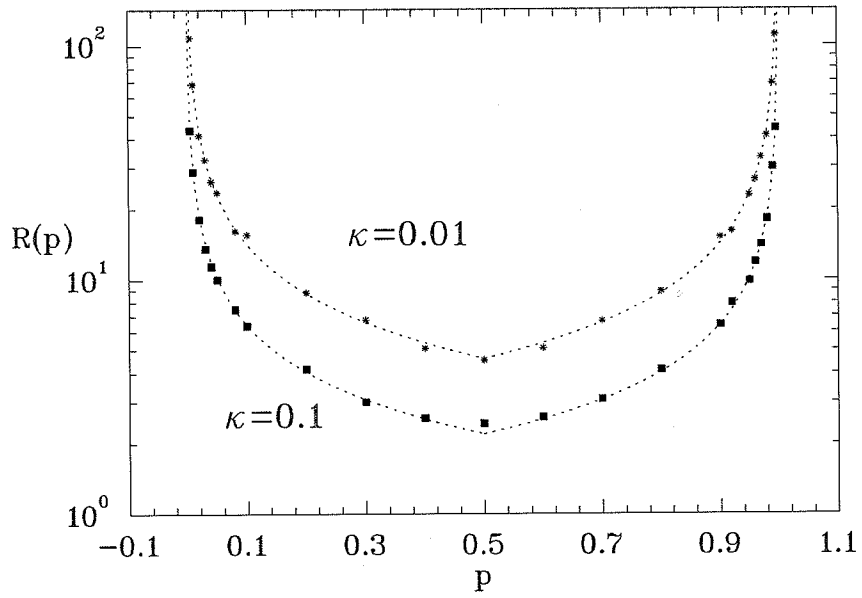

Figure 4. The ratio of the local-field moments, $R = M_4/(M_2)^2$ as a function of the metal coverage p, for two different values of the loss-factor κ (both values satisfy the inequality $\xi_e \ll aL$); the dashed lines represent fits based on Eq. (13).

onance condition for isolated silver particles is fulfilled at the wavelength $\lambda \approx 370$ nm. In Fig. 5, we see that the fluctuating local fields are well localized and enhanced with the enhancement of the order of 10^4 for $I(\mathbf{r})$, and 10^9 for $I^2(\mathbf{r})$. The spatial separation of the local peaks has a minimum when the wavelength of the applied filed corresponds to the single particle resonance. In this case, most of particles resonate and the local filed is enhanced randomly all over the film surface (Fig. 5a,b). With the increase of the wavelength, only few spatial regions can support propagation of plasmon modes which in turn leads to very high fields, significantly larger than those observed in the single particle resonance case. All these results support the assumption of plasmon localization in random metal-dielectric films and they are in qualitative agreement with the previously developed theory [4–8].

Based on similarities between the Kirchhoff's Hamiltonian $\hat{\mathbf{H}}$ and the quantum-mechanical Hamiltonian for the Anderson transition problem, the scaling theory predicts that there should be a power-law dependence for the

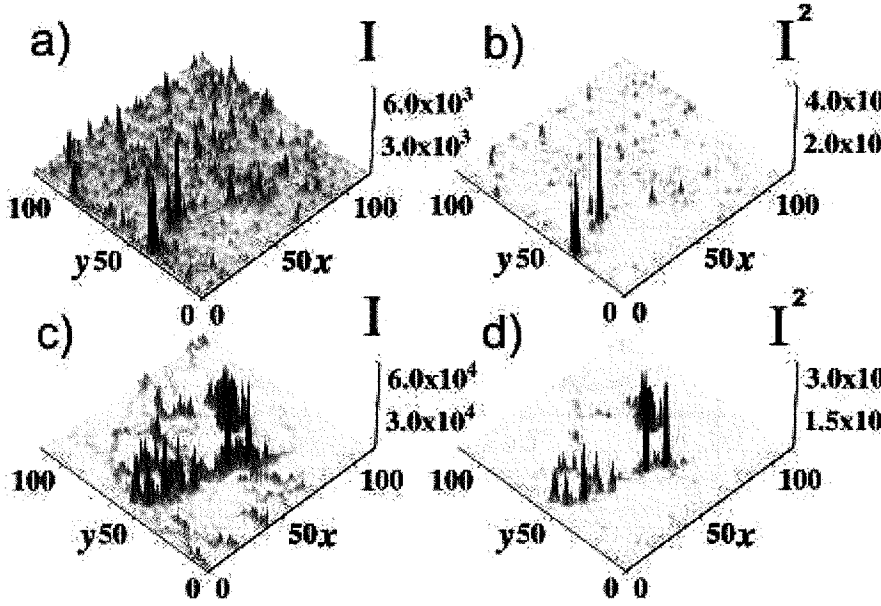

Figure 5. The spatial distributions of the normalized local intensity, $I(x, y)$, and the "local Raman enhancement factor", $I^2(x, y)$. The distributions are calculated at t different wavelengths: $\lambda = 0.370$ μm (a, b) and and $\lambda = 10$ μm (c, d). The metal fill factor is chosen as $p = p_c$ for all cases.

higher-order field moments:

$$M_n = \langle |\mathbf{E}|^n \rangle / |\mathbf{E}_0|^n \sim \int d\Lambda \frac{\rho(\Lambda)[a/\xi_f(\Lambda)]^{2n-d}}{[\Lambda^2 + \kappa^2]^{n/2}} \sim \kappa^{-n+1}, \qquad (1$$

where $n = 2, 3, 4, \ldots$, $\rho(\Lambda)$ is the density of states, $\xi_f(\Lambda)$ represents t average single mode localization length which corresponds to eigenvalue and κ is the loss factor [7]. This functional dependence was checked earli using the approximate real space renormalization group (RSRG) metho where qualitative agreement was accomplished with Eq. (14). Howev since the renormalization procedure is not exact, it is worth estimating t field moments with the exact BE method. To determine the field momer M_n, we used the BE procedure for surface filling fraction $p = p_c$ and κ $1 \div 10^{-3}$. Our results are shown on the log-log scale in Fig. 6. The da points represent a fit to a power law with each field moment having differe exponents.

For M_2 we obtained the exponent $x_2 = 1.0 \pm 0.1$, which is close to t one predicted by the scaling theory. For the third and the fourth momen we obtain that $M_{3,4} \sim \kappa^{-x_{3,4}}$, where the exponents $x_{3,4}$ are estimated

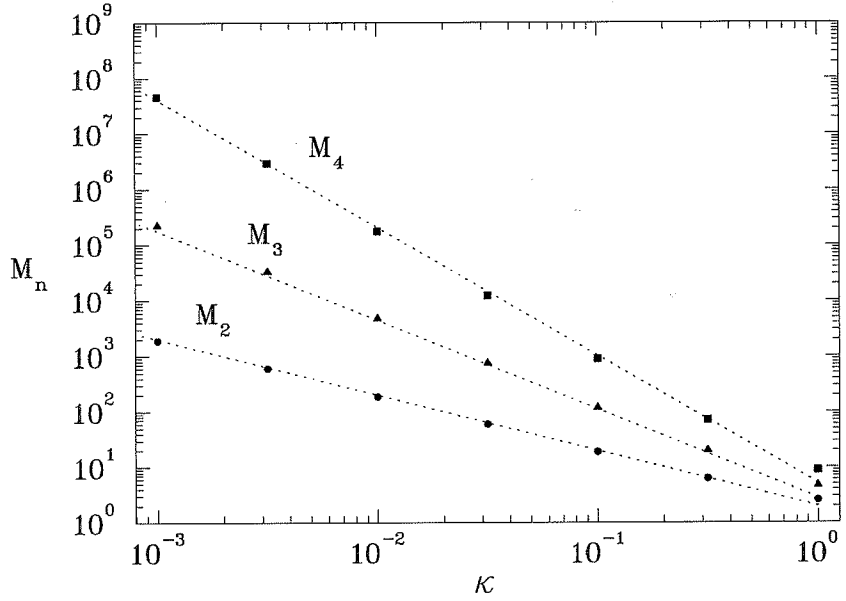

Figure 6. High-order field moments M_2, M_3, and M_4, as functions of the loss parameter κ; the calculations were performed for 100 different realizations in each case, for a lattice with size $L = 150$.

$x_3 = 1.7 \pm 0.1$, and $x_4 = 2.4 \pm 0.2$ which are somewhat different from the values predicted by Eq. (14): $x_3 = 2$ and $x_4 = 3$. This slight difference between the predicted and calculated values of the field moments exponents suggests the possibility of existence of non-localized or extended eigenmodes in the bond percolation model.

As we have mentioned above the scaling solution (14) is based on the assumption that the localization length $\xi_f(\Lambda)$ is finite for all Λ and it does not scale with the size of the system. If the function $\xi_f(\Lambda)$ has a pole, for example, at $\Lambda = 0$ (note that in the previous publications, we used the notation ξ_A for this case), this can lead to a change in the scaling indices, which is responsible for the difference above in the indices in Eq. (14) and those found from the exact numerical method. The minimum of the correlation length ξ_e at the percolation threshold and the log-normal distribution resulting from the strong coupling between the dipoles also suggest that at $\Lambda = 0$ we can expect localization-delocalization transition [10, 33]. To explicitly determine $\xi_f(\Lambda)$ we solve the eigenvalue problem for the real part $\hat{\mathbf{H}}'$ of the Kirchhoff's Hamiltonian $\hat{\mathbf{H}} = \hat{\mathbf{H}}' + i\kappa\hat{\mathbf{H}}''$ in $2D$. The eigenvalue problem was solved with *Mathematica* software for lattice sizes up to $L = 50$. In our calculations of the localization length we used the

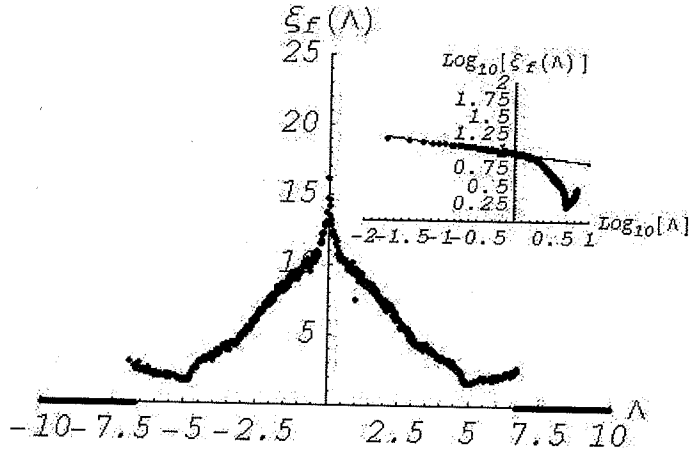

Figure 7. Localization length $\xi_f(\Lambda)$ as a function of the eigenvalues Λ calculated metal concentration equal to the percolation threshold p_c. The log-log inset depicts scaling region with an exponent $\chi \approx 0.14$.

inverse participation ratio so that for each eigenmode Ψ_n that satisfies equation $\hat{\mathbf{H}}'\Psi_n = \Lambda_n\Psi_n$, the localization length for n-th mode $\xi_f^{(n)}$ is gi by $\xi_f^{(n)} = [(\sum_{i,j}^N |\mathbf{E}_n(i,j)|^4)/(\sum_{i,j}^N |\mathbf{E}_n(i,j)|^2)^2]^{-1/2}$, where $\mathbf{E}_n = -\nabla$ Results for the average localization length $\xi_f(\Lambda)$ are shown in Fig. 7.

This figure illustrates that all states but $\Lambda = 0$ are localized as predic by the theory. Localization lengths are symmetrically distributed with spect to the zero eigenvalue and scale as a power law $\xi_f(\Lambda) \sim \Lambda^{-\chi}$ (t can be seen from the log-log inset). For the delocalization exponent we tain a value $\chi = 0.14 \pm 0.02$. By substituting the power law dependence the field localization length in Eq. (14) and performing the integration arrive at a new modified expression for the field moments in the form M_n $\kappa^{-n(1-\chi)+1}$. Using this equation we easily obtain new exponents x_3 and that have the values $x_3 = 1.58 \pm 0.06$ and $x_4 = 2.44 \pm 0.08$. These exp nents are in much better agreement with those found in the simulatio We note that although the presence of delocalized states at $\Lambda = 0$ resu in a slight change of the critical exponents in Eq. (14), all basic conclusic of the previously developed scaling theory still hold because the relati weight of the delocalized states is small.

The presence of non-localized states in random metal-dielectric fil was also investigated by Stockman, Faleev and Bergman [10]. While t results we have presented are in qualitative agreement with Ref. [10], is difficult to compare them quantitatively. This difficulty arises from t fact that in the calculations of the localization length

rely on the gyration radius. However, for eigenstates consisting of two (or more) spatially separated peaks, the gyration radius is characterized by the distance between the peaks rather than by the spatial sizes of individual peaks, which can be much smaller than the peak separation. In contrast, the inverse participation ratio used above characterizes sizes of individual peaks. We note that namely thus defined quantity ξ_f enters Eq. (14) and other formulas of the scaling theory.

6. Discussion and Conclusions

In this paper we introduced a new numerical method which we refer to as block elimination (BE). The BE method takes advantage of a block structure of the Kirchhoff Hamiltonian $\hat{\mathbf{H}}$ and thus decreases the amount of numerical operations and memory required for solving the Kirchhoff equations for square networks. Note that this method is exact as opposed to previously used numerical methods, most of which are approximate. The results obtained show that the BE method reproduces well the known critical exponents and distribution functions obtained by other methods. The BE verifies the large enhancement of the local electric field predicted by the earlier theory [4–8]. Specifically, the BE results are in good accord with the estimates following from the real space renormalization group.

Besides suggesting a new efficient numerical method, we thoroughly examined the local field distribution function $P(I)$ for different metal filling factors p and loss factors κ. The important result here is that in the optical and infrared spectral range, the local electric field intensity is distributed over an exponentially broad range; specifically, the function $P(I)$ can be characterized by the log-normal function. The latter result, however, holds only in a close vicinity of the percolation threshold and for the light frequencies close or equal to the surface plasmon resonance of individual metal particles. For metal concentrations far away from the percolation region, a power-law behavior was found for $P(I)$. This "scaling" tail in the local field distribution can be related to the one-dipole distribution function. The BE method also verifies the localization of plasmons predicted earlier by the scaling theory. The ensemble average high-order moments for the local field have also been calculated. We found a power law exponents that are in qualitative accord with the scaling theory. With the introduction of corrections due to the presence of extended eigenmodes in the KH we obtained very good agreement between theory and simulations.

Acknowledgement

This work was supported by Battelle under contract DAAD19-02-D-0001, NASA (NCC-1-01049), ARO (DAAD19-01-1-0682), and NSF (E SC-02104

45).

Appendix

In this Appendix we outline the construction of the KH in terms bond conductivities. As we show in Section 2, the Kirchhoff equati the quasistatic approximation provide solutions for the field distribut a composite medium. We consider the construction of the matrix E for the two-dimensional case (the three-dimension procedure is anal and treat a metal-dielectric film as a square lattice of size L. Th potentials at the sites of the lattice are described by vector $\{\varphi_i\}$, $i = 1, 2, \ldots, L^2$. All sites are connected by conducting bonds $\sigma_{i,j}$, index $j = \{i-1, i+1, i+L, i-L\}$ includes all the nearest neighb site i. Then, we can re-write Eq. (1) in the following form:

$$-\frac{1}{\Delta}[\sigma_{i,i+1}(\varphi_{i+1}-\varphi_i)-\sigma_{i,i-1}(\varphi_i-\varphi_{i-1})]+E_{0x}(\sigma_{i,i+1}-\sigma_{i,i-1})$$
$$-\frac{1}{\Delta}[\sigma_{i,i+L}(\varphi_{i+L}-\varphi_i)-\sigma_{i,j-L}(\varphi_i-\varphi_{i-L})]+E_{0y}(\sigma_{i,i+L}-\sigma_{i,i-L})=$$

where $\Delta = a = 1/L$ is the bond length and the pair (E_{0x}, E_{0y}) repr the components of the applied electric field. We can rewrite Eq. (15 slightly different way:

$$h_{i,i}^{(jj)}\varphi_{i+(j-1)L}+h_{i,i+1}^{(jj)}\varphi_{i+(j-1)L+1}+h_{i,i-1}^{(jj)}\varphi_{i+(j-1)L-1}$$
$$+h_{i,i}^{(j,j+1)}\varphi_{i+jL}+h_{i,i}^{(j-1,j)}\varphi_{i+(j-2)L}=F_i^{(j)},$$

where $i' = i + (j-1)L$. If $L < i' < L^2 - L$, the components of ma $h^{(ij)}$ and vectors $F^{(j)}$ can be written as $h_{i,i}^{(jj)} = \sigma_{i',i'+1}+\sigma_{i',i'-1}+\sigma_{i',i}$ $\sigma_{i',i'-L}$, $h_{i,i+1}^{(jj)} = -\sigma_{i',i'+1}$, $h_{i,i-1}^{(jj)} = -\sigma_{i',i'-1}$, $h_{i,i}^{(j,j+1)} = -\sigma_{i',i'+L}$, $h_{i,i}^{(j-}$ $-\sigma_{i',i'-L}$, and $F_i^{(j)} = -\Delta\,[E_{0x}(\sigma_{i',i'+1}-\sigma_{i',i'-1})+E_{0y}(\sigma_{i',i'+L}-\sigma_{i',i}$ The elements in the first and the last rows of matrix $\hat{\mathbf{H}}$ in Eq. (4), ever, must be described in accordance with the boundary conditions. parallel boundaries (zero on the bottom and unity on the top) are then $h_{i,j}^{(11)} = h_{i,j}^{(LL)} = \delta_{ij}$; for the periodic boundary conditions, the m elements are described by relations similar to Eq. (3). We should poi that for the periodic boundaries, the matrix $\hat{\mathbf{H}}$ has rank $L^2 - 1$, a order for the system to have a solution, one of the site potentials mu grounded.

References

1. W.L. Mochan and R.G. Barrera, *Physica A* **241** (1997), 1–452 .
2. D.J. Bergman and D. Stroud, *Solid State Physics* **46** (1992), 147–269.
3. A.K. Sarychev, *Zh. Eksp. Teor. Fiz.* **72** (1977), 1001–1006.
4. V.M. Shalaev and A.K. Sarychev, *Phys. Rev. B* **57** (1998), 13265–13288.
5. A.K. Sarychev, V.A. Shubin, and V.M. Shalaev, *Phys. Rev. B* **60** (1999), 16389–16409.
6. A.K. Sarychev, V.A. Shubin and V.M. Shalaev, *Phys. Rev. E* **59** (1999), 7239–7242.
7. A.K. Sarychev and V.M. Shalaev, *Physics Reports* **335** (2000), 275–371.
8. V. M. Shalaev, *Nonlinear Optics of Random Media: Fractal Composites and Metal-Dielectric Films*, Springer Tracts in Modern Physics v. 158, Springer, Berlin, Germany, 2000.
9. S. Gresillon, L. Aigouy , A.C. Boccara, J.C. Rivoal, X. Quelin, C. Desmarest, P. Gadenne, V.A. Shubin, A.K. Sarychev and V.M. Shalaev, *Phys. Rev. Lett.* **82** (1999), 4520–4523.
10. M.I. Stockman, S.V. Faleev and D.J. Bergman, *Phys. Rev. Lett.* **87** (2001), 167401–167404.
11. D.J. Frank and C.J. Lobb, *Phys. Rev. B* **37** (1988), 302–307.
12. L. Tortet, J.R. Gavarri, J. Musso, G. Nihoul, J.P. Clerc , A.N. Lagarkov and A.K. Sarychev, *Phys. Rev. B* **58** (1998), 5390.
13. A.K. Sarychev and A.P. Vinogradov, *J. Phys. C: Solid State Phys.* **14** (1981), L487–L490 .
14. J.P. Clerc, V.A. Podolskiy, A.K. Sarychev, *Europhys. J. B* **15** (2000), 507–516.
15. B. Derrida and J. Vannimenus, *J. Phys. A: Math. Gen.* **15** (1982), L557–L564.
16. S. Kirkpatrick, *Phys. Rev. Lett.* **27** (1971), 1722–1741.
17. G.G. Bartrouni, A. Hansen, and M. Nelkin, *Phys. Rev. Lett.* **57** (1986), 1336–1339.
18. L. Zekri, R. Bouamrane and N. Zekri, *J. Phys. A: Math. Gen.* **33** (2000), 649–656.
19. D.A. Genov, A.K. Sarychev and V.M. Shalaev, *Phys. Rev. E* (2002) (submited).
20. R. Coult et al., *Computational Methods in Linear Algebra,* John Wiley & Sons, New York, 1975.
21. V. Privman, *Finite-Size Scaling and Numerical Simulations of Statistical Systems,* World Scientific, Singapore, 1988.
22. D. Stauffer and A. Aharony, *Introduction to Percolation Theory,* 2nd Edition, Taylor and Francis, London, 1992.
23. F. Brouers, S. Blacher and A. K. Sarychev, *Phys. Rev. B* **58** (1998), 15897–15907.
24. J. Cardy, *Finite-Size Scaling,* North Holland, Amsterdam, 1981.
25. A. Aharony, R. Blumenfeld and A.B. Harris, *Phys. Rev. B* **47** (1993), 5756–5769.
26. B. Kramer and A. MacKinnon, *Rep. Prog. Phys.* **56** (1993), 1469–1564.
27. L. Zekri, R. Bouamrane, N. Zekri and F. Brouers, *J. Phys.: Cond. Matter* **12** (2000), 283–291.
28. E.D. Palik (Ed.), *Hand book of Oprical Constants of Solids,* Academic Press, New York, 1985.
29. V.A. Markel, V.M. Shalaev, E.B. Stechel, W. Kim and R.L. Armstrong, *Phys. Rev. B* **53** (1996), 2425,-2436.
30. M.I. Stockman, N.L. Pandey, L.S. Muratov and T.F. George, *Phys. Rev. Lett.* **72** (1994), 2486–2489.
31. S. Bozhevolnyi and V. Coello, *Phys. Rev. B* **64** (2001), 115414–115421.
32. Katayayani Seal, M.A. Nelson, Z.C. Ying, D.A. Genov, A.K. Sarychev and V. M. Shalaev, *Phys. Rev. B* (2002) (submited).
33. K. Müller, B. Mehling, F. Milde and M. Schreiber, *Phys. Rev. Lett.* **78** (1997), 215–218.

CHAPTER V

RADIATIVE TRANSFE

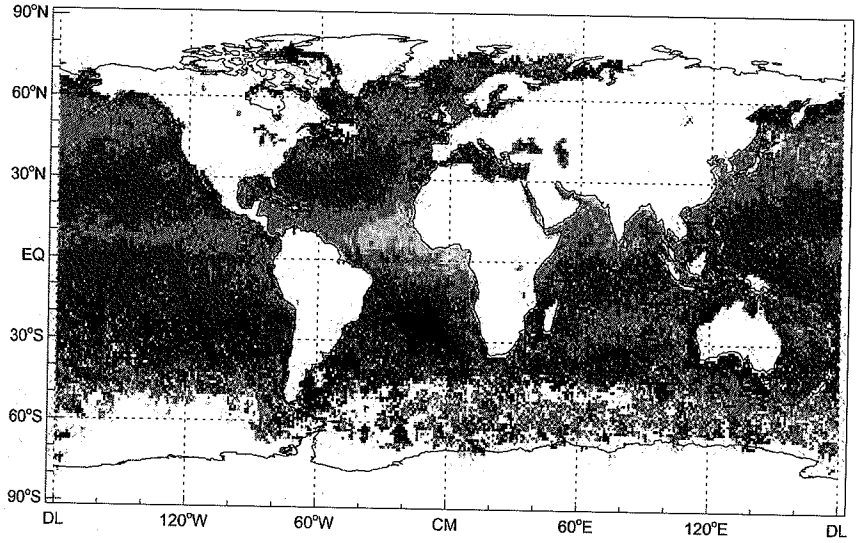

Global map of aerosol optical thickness averaged over the months of Feb July 2000. The results are retrieved from channel 1 and 2 radiances m by the Advanced Very High Resolution Radiometer on board of NOAA u satellites. The data are not available over the land as well as over area extensive cloud coverage (these areas are left white). The details of the re process are described in the paper M.I. Mishchenko, I.V. Geogdzhayev, B. C W.B. Rossow, and A.A. Lacis (1999) Aerosol retrievals over the ocean by channels 1 and 2 AVHRR data: sensitivity analysis and preliminary results, Opt. 38, 7325-7341. Image courtesy of Igor Geogdzhayev and Michael Mishc Goddard Institute for Space Studies, New York, USA.